

Article

Effects of Groundwater Inputs to the Hydraulic Circulation, Water Residence Time, and Salinity in a Moroccan Atlantic Lagoon

Soukaina Elyaagoubi ^{1,*} , Georg Umgieser ^{1,2} , Mehdi Maanan ³, Francesco Maicu ^{2,4}, Jovita Mėžinė ¹ , Karim Hilmi ⁵  and Artūras Razinkovas-Baziukas ¹

¹ Marine Research Institute, Klaipėda University, 92294 Klaipėda, Lithuania; georg.umgiesser@ismar.cnr.it (G.U.); jovita.mezine@ku.lt (J.M.); Arturas.Razinkovas-Baziukas@ku.lt (A.R.-B.)
² Institute of Marine Sciences, ISMAR CNR, 30122 Venice, Italy; francesco.maicu@unibo.it
³ Faculty of Sciences Ain Chock, University Hassan II, Casablanca 20000, Morocco; mehdi.maanan@gmail.com
⁴ Department of Physics and Astronomy, University of Bologna, 40127 Bologna, Italy
⁵ INRH Institut National de Recherche Halieutique, Casablanca 20180, Morocco; karimhilmi15@gmail.com
* Correspondence: soukaina.elyaagoubi@apc.ku.lt

Abstract: The finite element model SHYFEM was used to study the hydrodynamics and variability of water level, salinity, temperature, and water residence time (WRT) in the Oualidia lagoon located on the Moroccan Atlantic coast. The lagoon hosts a RAMSAR convention-protected area and also offers a set of valuable ecosystem services providing the source of income for the local population. To assess the effects of submarine groundwater discharge (SGD) inputs in the study area, four simulations were set up using different SGD inputs estimates in addition to tidal forcing, bathymetry, meteorological data including solar radiation, rain, and wind, in addition to boundary conditions in the Atlantic such as salinity, water level, and water temperature. The model was calibrated and validated using hydrodynamic measurements of previous studies in 2012 and 2013. The final results from the model are in good agreement with measured data. The simulation with SGD input $\sim 0.05 \text{ m}^3 \text{ s}^{-1}$ produced salinity values closest to the observed ones. Calculated spatial distribution of WRT, temperature, and salinity reduced to coordinates in two PCA axes is consistent with lagoon zones developed earlier using the benthic macroinvertebrate distribution. The calculated spatial distribution of WRT allowed us to evaluate the placement of oyster aquaculture farms and small-scale fisheries in relation to water quality issues existing in the lagoon.

Keywords: finite element modeling; SHYFEM; hydrodynamics; SGD inputs; physical parameters; coastal ecosystem; shallow coastal lagoon; oualidia lagoon; ecosystem services



Citation: Elyaagoubi, S.; Umgieser, G.; Maanan, M.; Maicu, F.; Mėžinė, J.; Hilmi, K.; Razinkovas-Baziukas, A. Effects of Groundwater Inputs to the Hydraulic Circulation, Water Residence Time, and Salinity in a Moroccan Atlantic Lagoon. *J. Mar. Sci. Eng.* **2022**, *10*, 69. <https://doi.org/10.3390/jmse10010069>

Academic Editor: Rafael J. Bergillos

Received: 26 November 2021

Accepted: 3 January 2022

Published: 6 January 2022

Publisher's Note: MDPI stays neutral with regard to jurisdictional claims in published maps and institutional affiliations.



Copyright: © 2022 by the authors. Licensee MDPI, Basel, Switzerland. This article is an open access article distributed under the terms and conditions of the Creative Commons Attribution (CC BY) license (<https://creativecommons.org/licenses/by/4.0/>).

1. Introduction

Coastal lagoons are considered as the most important life and human wellbeing provider areas in both terrestrial and water body parts. They are the most highly productive coastal features as their ecosystem offers a decently valuable natural benefit, ecologically, culturally, and socioeconomically [1]. The lagoon of Oualidia is a shallow saltwater estuary, maintained by fresh SGD inflow [2–4]. It can be described as an important system that offers a trove of natural wealth despite its relatively small size of 7 km long and 1 km wide. The lagoon is highly exploited by human activities such as tourism, fisheries, and aquaculture, mainly oyster farming that can reach 250 tons of production per year. The lagoon has been one of the most important oyster farming areas since 1950, and for this reason, it has been called the “traditional oyster capital” in Morocco [5–7].

To support the sustainable and effective use of these natural resources, it is necessary to assess the present hydraulic circulation patterns and also classify the lagoon into different hydraulic circulation zones. The model would also be critical for assessing the future

changes expected due to climatic changes in both the terrestrial parts of the Moroccan Atlantic coast and the Atlantic Ocean.

In the case of coastal lagoons, numerical models have been utilized to offer a better understanding of the underlying physical patterns dictating the consequences induced by altering their key properties, including their isolation degree. For example, numerical models have been frequently applied to represent the water exchange between the lagoons and open sea or other coastal bodies, given its relevance for numerous biogeochemical and ecological processes [8].

Numerical modeling using finite element approaches in hydrodynamics is considered as a flexible way to represent complicated bathymetry because of the scalable triangulated net, especially suitable for shallow areas as coastal lagoons but not excluding deeper areas [9].

Previously studied in a different site [10], the findings of field measurements as well as their reaction using a 3D numerical model of the lagoon were given. Their study makes use of reconstructed bathymetry, water volume, tides, water residence time, salinity, and freshwater inputs.

Over the last decade, SGD-seawater interactions, in addition to riverine inputs, have gotten a lot of interest while studying the coastal zone process. The SGD in the lagoons in arid areas where precipitation is low is always important to both the distribution of physical and chemical characteristics as temperature, salinity, oxygen, and nutrient concentrations as they constitute a substantial part of freshwater inputs. As SGD has been demonstrated to provide considerable quantities of nutrients to lagoons and coastal water bodies [11–13]; the amount of groundwater draining into lagoons might range from small contributions to major ones [14,15].

Multiple variables impact coastal underground groundwater flow dynamics and SGD, which vary on temporal and geographical scales, resulting in a complex subsurface flow system [13]. WRT is also an essential characteristic that is frequently difficult to quantify. In fact, many of the physical and ecological processes in coastal lagoons and estuaries are controlled by the WRT, which includes the biochemical cycles and other important ecosystem functions [16,17].

Such efforts in numerical modeling are intended to serve as a foundation for additional in-depth studies on hydrodynamics and hydraulic characteristics of the investigated water body [10]. Moreover, hydraulic circulation is critical for the majority of physical and biogeochemical activities in coastal and lagoon ecosystems [18]. Additionally, mathematical models are very useful to evaluate not only hydrodynamics, but also ice dynamics and its forcing on the coast of the study site as in [19].

The paper describes the steps toward the application of the SHYFEM model in the Oualidia lagoon to describe the physical forcing important for the ecosystem function and services, taking into consideration the SGD and their possible effects on the hydraulic circulation.

2. Materials and Methods

2.1. Study Area

Oualidia is a western Moroccan lagoon connected to the Atlantic through two inlets. The major pass is 150 m wide and 2 m deep. The lagoon has been designated to be of international importance; it has been under the international wetland's convention RAMSAR since 2005 [5,20]. The lagoon has an elongated shape composed of channels (Figure 1) where the main channel is in the NE-SW direction and can reach 5 m depth during flood tides with a 2 m average [3,4,21]. The climate in Oualidia is dry to half-dry. Generally, in the summer season, the atmospheric temperature is around ~ 36 °C, while in the winter season, it is around ~ 15 °C [22]. Authors have mentioned that hydrologically the lagoon depends significantly on the tidal regime [3,4,23].

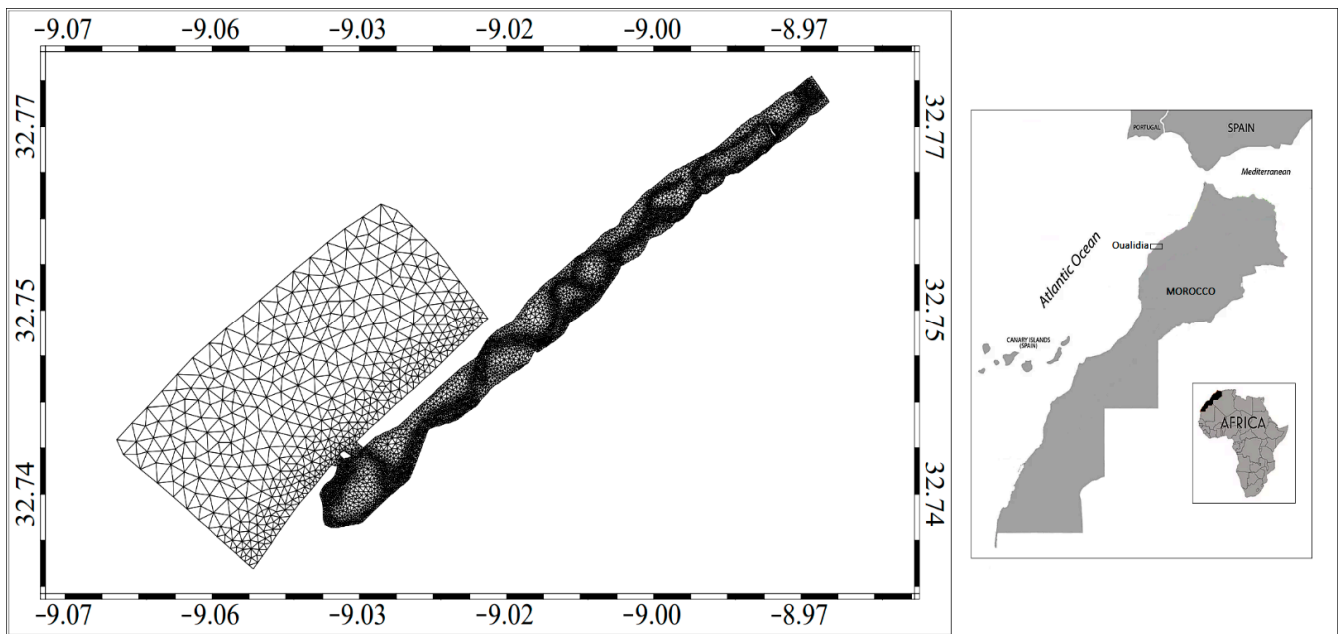


Figure 1. Grid of the study area ‘Oualidia’ lagoon and its location.

The water temperature of the lagoon is between 16 and 25 °C, going from downstream to the inner part in spring, considering the downstream as the entrance, knowing that the inlets are located in that part of the lagoon. Water temperature decreases according to the 1. 18 °C · km⁻¹ gradients. Salinity varies from 22.5 and 35.9 mg · L⁻¹ in the summer season with an average of 33 mg · L⁻¹ [24]. The lagoon has a significant increase in organic production, which favors aquaculture improvement due to the nutrient input during high tides; also it varies according to the season and the location [5]. In the spring/summer period, a maximum of NO_x concentrations can reach 18.3 μmol · L⁻¹ in the inner part of the lagoon, while the minimum can be 0.02 μmol · L⁻¹ in downstream with an average of 5.52 μmol · L⁻¹. The maximum and minimum concentrations of orthophosphate in the water of the lagoon are respectively 89.4 μmol · L⁻¹ in the middle and 0.1 μmol · L⁻¹ in the downstream [24].

Oualidia lagoon supports human welfare for the local inhabitants, which were ~18,616 in 2014. There are seven aquaculture farms in total in the lagoon, which produce yearly ~250 tons of oysters. The small-scale fishery and coastal resources collection are also considered as highly important activities practiced by locals seasonally. In addition to recreational fishing, fishermen use artisanal boats and go sailing seven times a week for 5–8 h per trip; they are active almost all along the year [25].

2.2. Data

Data used for this numerical investigation are (1) an orthophoto of a 40 × 40 cm spatial resolution (Figure 2), (2) a detailed topo bathymetric survey inside the lagoon was carried out by echo-sounding, and bathymetric data of the boundary area in the ocean part was downloaded from the general bathymetric chart of the ocean’s platform GEBCO. In addition, (3) meteorological forcings, which are mainly the heat fluxes, rain, and wind, they were obtained as NETCDF files by the European Centre for Medium-Range Weather Forecasts (ECMWF, <http://www.ecmwf.int> (accessed on 19 April 2019)).

The boundary conditions data used for the simulations are salinity, water levels, and temperature. These were downloaded according to the period of simulations from the reanalysis of the IBI model product in the Copernicus project. <http://marine.copernicus.eu/services-portfolio/access-to-products/> (accessed on 5 January 2022).

For the model’s performance validation by harmonic analysis, phase and amplitude measurements of tidal water levels were gathered at five stations (Figure 2) throughout

the lagoon channel beginning at the entrance; their geographical distributions are given in (Table 1). The tide gauge, current meter, and CTD diver tools were used to make the measurements in 2012; data source (DPDPM/MET, 2012). (Table 1) shows the precise coordinates of each station, the predicted water depth at the time of measurement, and the instruments and their sensor height.

Data for validation of salinity were extracted from 42 stations sampled in the previous study [26]. The salinity in this previous work was recorded for the month of March 2013. Therefore, it was used for comparison to the model’s results for the same period, taking into consideration the SGD discharges. The choice of nodes that represents the estimated locations of SGD sources was based on the study of [2], where the discharge of SGD in the lagoon was identified. (Figure 2).

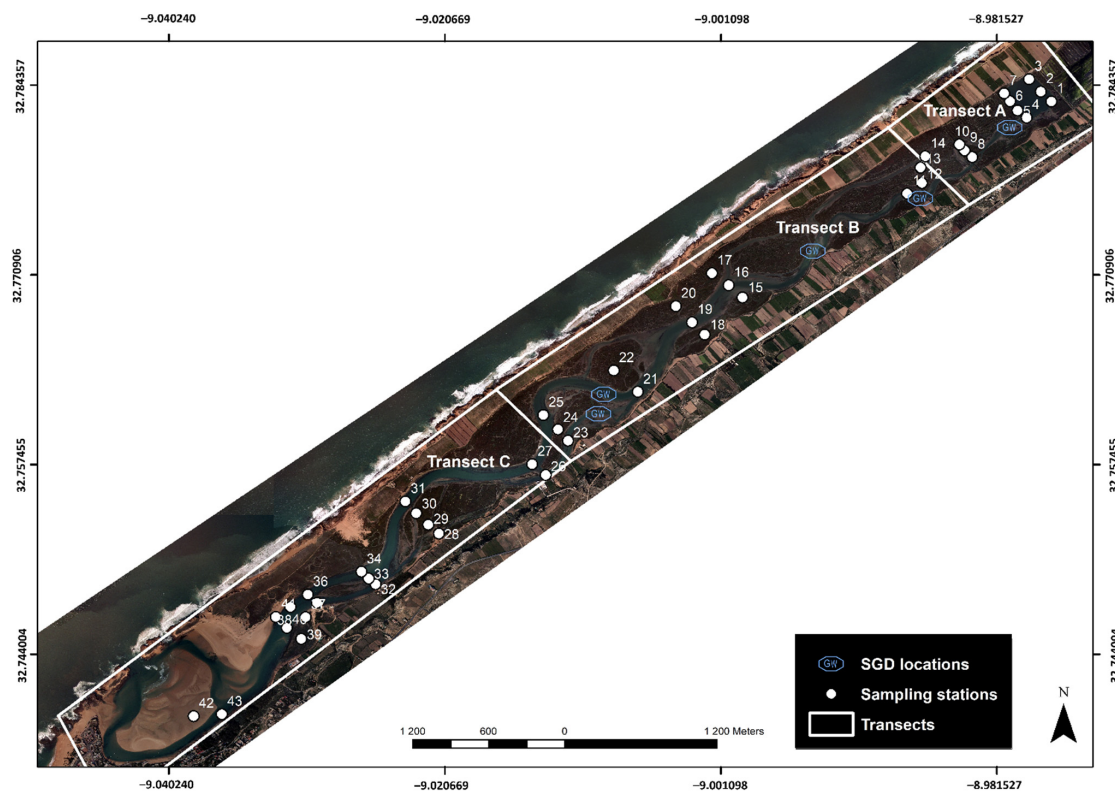


Figure 2. Orthophoto, 42 sampling stations [26], transects distribution (A, B, C), SGD locations [2] and tide gauges positions (1–5).

Table 1. Stations spatial distribution, depth, and measurements instruments for harmonic analysis (Source DPDPM/MET, 2012).

Stations	Position X	Position Y	Depth	Tool/Instrument	Sensor Height
1	495,466	3,622,202	−5.05 m	Tide gauge	0.27 m
				Current meter	0.22 m
2	496,883	3,622,553	−2.17 m	CTD	0.11 m
				Tide gauge	0.24 m
				Current meter	0.14 m
3	498,873	3,624,787	−2.20 m	CTD	0.11 m
				Current meter	0.14 m
4	500,324	3,625,534	−2.06 m	Current meter	0.14 m
5	501,683	3,626,651	−0.89 m	Tide gauge	0.24 m
				CTD	0.08 m

2.3. Model

In this study, we have applied SHYFEM (System of Hydrodynamic Finite Element Modules; <https://github.com/SHYFEM-model/shyferm> (accessed on 14 December 2021)), a hydrodynamic model for shallow water environments utilizing the finite element approach that is highly convenient for complicated areas geometry, and very suitable for a spatial resolution use and a semi-implicit algorithm for time integration (Figure 3) [27]. An open-source code that has been developed at ISMAR-CNR (Institute of Marine Science—National Research Council, www.ismar.cnr.it/shyferm (accessed on 17 November 2021)) [9]. SHYFEM is a 3-D hydrostatic model that solves the primitive equations integrated vertically over each z layer and horizontally over an unstructured triangular finite element mesh [17]. The SHYFEM model was successfully used for shallow water environments in several works since 1973, it also was applied to model tides and even to deeper zones using 3D modeling [28,29].

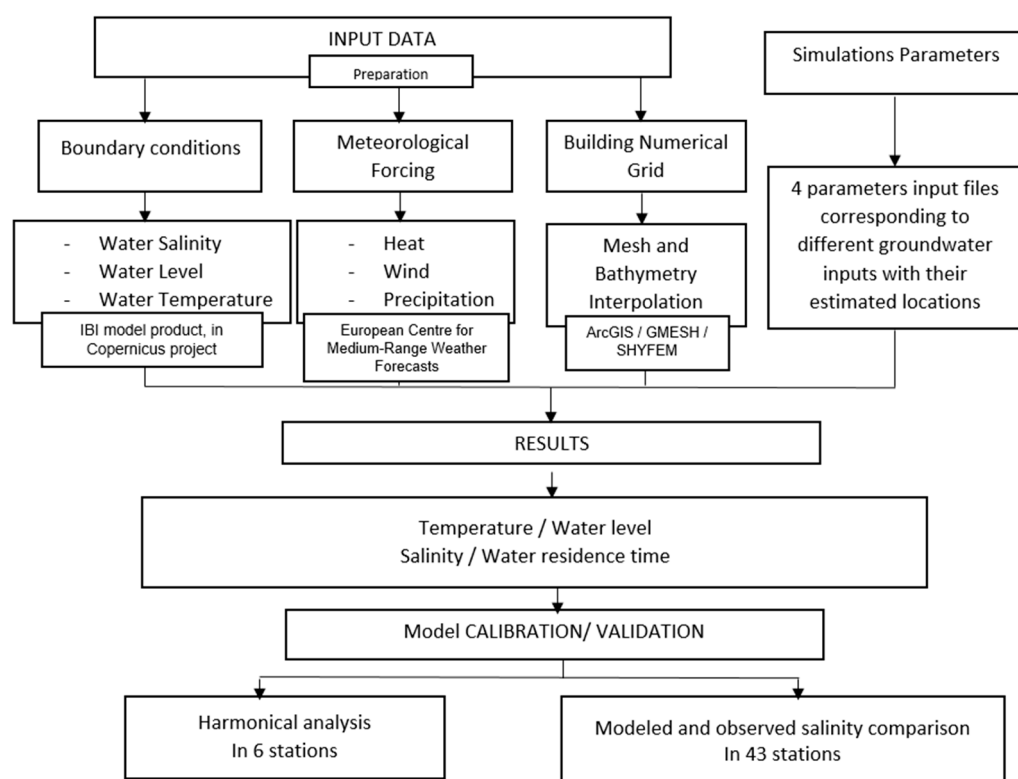


Figure 3. Framework/Methodology.

Also, in terms of hydrodynamics and water exchange, the model has been applied and gave satisfying results on several lagoons, and more details can be found in a comparative article that accumulates numerical hydrodynamic modeling in ten Mediterranean lagoons [17]. Several applications to lagoons are shown, and recently [30], this model has been applied on the Lagoon of Nador (Morocco) to assess the changes of the hydrodynamics after the inlet modification. The time integration of the equations uses a semi-implicit scheme and a staggered grid to conserve the water mass, with water levels and other scalar variables calculated at the vertices, while velocities are calculated at the centers of the elements using a step shape function.

The 3D advection–dispersion processes of scalars are solved with a second-order explicit total variance diminishing (TVD) scheme [31]. It uses the GOTM turbulence closure scheme for the description of vertical turbulence [30], and the horizontal turbulence is handled with the Smagorinsky approach [32]. In the case of salinity, the difference between evaporation and rainfall through the water surface is considered. Water temperature is

computed through the heat flux between the atmosphere and the sea by the balance of the energy radiation with latent and sensible heat fluxes [33].

The advection–diffusion module applied to a passive tracer, allowing the calculation of the WRT [34], which can be considered a general descriptor of the lagoon dynamics that takes into account both hydrodynamics and mixing (advection and dispersion). According to the definition of [35], the WRT is calculated, in each node of the numerical grid, as the time needed to lower the concentration of the passive tracer from 1 to $1/e$. At the beginning of the simulations, the tracer concentration is set to one inside the lagoon and zero outside. Then, the tracer propagates and can leave and re-enter the lagoon, while it is removed only when it crosses the open boundary. In this investigation, the SHYFEM model required firstly building a numerical grid of the study area (Figure 1). The mesh was built using GMesh software, then converted to the model format. Our grid is made of 6157 nodes and 11,631 triangular elements that vary in form and size depending on the areas of high or low interest along our study area. The elements that compose the grid represent and reproduce the topography of the investigated area. A higher number of triangular elements, which automatically represent the higher resolution, are mainly located in inlets that connect the lagoon with the Atlantic Ocean and the channels. These surfaces were chosen to be represented with higher resolution due to their importance in this study case for better modeled results. A medium resolution is applied on sand and salt marshes, and finally, the outer oceanic part is represented with lower resolution (less triangular elements). Then, the interpolation of the existing bathymetry onto the grid is carried out. The channel depth is around 5 m as a maximum value, the sand and dunes are quite shallow from 0 to 1 m, and in the boundary, the depth along the coastline increases from 5 to 9 m and over 10 m further in the ocean. The lagoon boundary is the Atlantic coastline; it is highly affected by the ocean tides.

The model simulation has been carried out for the time period from 1st January 2010 until the end of December 2014; however, as the calibration data were available only for the spring of 2013.

Four simulations were run in this study using different estimated SGD inputs in each, 0 (no SGD input), 0.2, 0.1, and 0.05. The main objective was to see which is in best agreement with the observed salinity in 42 stations (Figure 2), referring to the study carried out by [26].

3. Results

3.1. Calibration and Validation

3.1.1. Harmonic Analysis

Harmonic analysis is essentially the process of computing the amplitudes and phases of a limited number of sinusoidal functions with known frequencies. The harmonic approach of tidal analysis demonstrates that the astronomical forcing for tides may be expressed as a linear combination of sinusoidal components with different amplitude, phase, and temporal frequency. The oceanic reaction to this force may be described similarly, with each sinusoid denoted by the term tidal component. While the component frequencies are identical to those of the tidal potential, the constituents' amplitudes and phases may vary significantly owing to the uneven coastline limits and bathymetry of the earth's seas. All tidal frequencies are linear combinations of frequencies referred to as harmonics [36]. For each of the five stations from (Table 1), a comparison of the predicted and observed findings was performed; (Table A1) and graphs below in (Figure 4) provide more information.

Station 1: This station is located approximatively near the inlet of the lagoon. The modeled phase and amplitude were compared to the previously measured ones for 19 waves (Table A1). The comparison outcome is well presented in the histograms in (Figure 4a,b). Regarding the phase for this station, values of measured and modeled results are in disagreement in certain waves like (NO1, MU2, L2, MK3, SN4, M6, 2MS6) (Figure 4a), while the modeled and measured amplitude results are perfectly in agreement in all the 19 waves (Figure 4b).

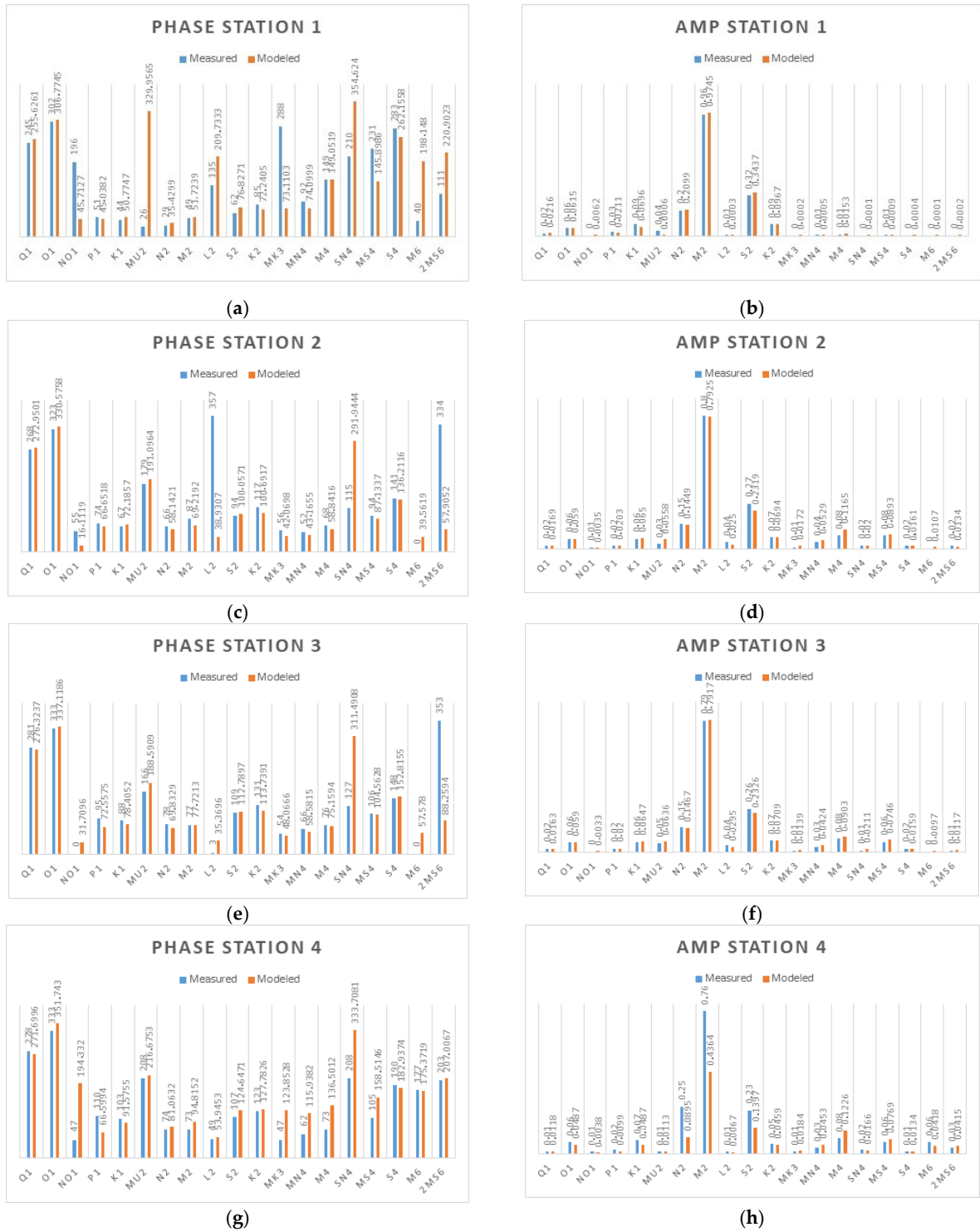


Figure 4. Cont.



Figure 4. Histograms for modeled results for Phase (degrees) and Amplitude (meters) in comparison with the measured. (a) Phase S1; (b) Amplitude S1; (c) Phase S2; (d) Amplitude S2; (e) Phase S3; (f) Amplitude S3; (g) Phase S4; (h) Amplitude S4; (i) Phase S5; (j) Amplitude S5.

Station 2: This station is positioned in front of the lagoon’s entrance from the opposite side of the S1. For 19 waves, the simulated phase and amplitude were compared to previously recorded ones, the same way for the previous station and the upcoming ones. For this station, the second column of (Table A1). The phase results comparison of modeled and measured in this station are in agreement in most of the waves except for almost the same waves that have a disagreement in the S1, mainly (NO1, L2, SN4, M6, 2MS6) (Figure 4c). While the amplitude values from the model and the measurements coincide precisely in all 19 waves, identical as S1 (Figure 4d).

Station 3: The S3 is located in the middle of the lagoon on the channel side next to the coastline. Results of compared modeled and observed phase and amplitude are shown in the third column of (Table A1). In the phase, mainly the result’s comparison is accurate for most of the components, except for a few waves (NO1, L2, SN4, M6, 2MS6) out of 19 (Figure 4e). While the model and observations agree exactly on the amplitude values for all 19 waves, the same way as for S1 and S2 (Figure 4f).

Station 4: This station is located at the beginning of the inner part of the lagoon coming from the middle part. It is on the channel part that is closer to the terrestrial side. The fourth column of (Table A1) shows the values for the phase and amplitude of the model results and observations. In comparison with the previous stations (1, 2, and 3), the phase in this station has fewer components in disagreement between model and observations (NO1, SN4, MS4) out of 19 waves (Figure 4g). Meanwhile, the amplitudes of the modeled waves are as accurate as in the previous stations, except for one wave (M2) out of the 19 given waves (Figure 4h).

Station 5: The fifth and last station is located approximately in the very inner part of the lagoon, considering the inlets as the beginning. The last column of (Table A1) represents the outcome of phase and amplitude modeled and observed values. In this station, the modeled phase seems to be in agreement with the observations for all 19 waves (Figure 4i). Same as for the amplitude except for one wave (M2) with a difference estimated as ~0.2 m (Figure 4j).

Regarding the tidal modeling, stations 1–3 (Figure 2) show a very good correlation between measured and modeled results. Discrepancies show up mainly in very low amplitude tidal. However, stations 4 and 5 are more difficult to model, probably due to the large shallow areas and salt marshes. Here, bathymetry probably plays a crucial role; therefore, newer data is needed.

3.1.2. Validation of SGD Estimation

Results of the average modeled salinity for March 2013, in the three transects of the lagoon A, B, and C, of the four simulations of different estimated SGD inputs 0, 0.05, 0.1, and 0.2 m³ s⁻¹ are compared to the observed results and presented below (Table 2). The Root Mean Square Error (RMSE) was calculated for each estimated SGD input. The best

RMSE value (1.26) was found when the SGD was $0.05 \text{ m}^3 \text{ s}^{-1}$. This was the most accurate estimation and is in good agreement with the observed values along with the 42 stations (Figure 5B).

Table 2. Modeled salinity with different estimated SGD inputs and observed in the three transects of the lagoon and root mean square error RMSE for each.

Transects	SGD 0	SGD 0.05	SGD 0.1	SGD 0.2	Observation
A	33.66	29.97	27.74	24.23	31.77
B	34.83	33.22	32.12	30.24	32.53
C	35.56	35.20	34.95	34.44	36.21
RMSE	1.76	1.26	1.90	3.87	-

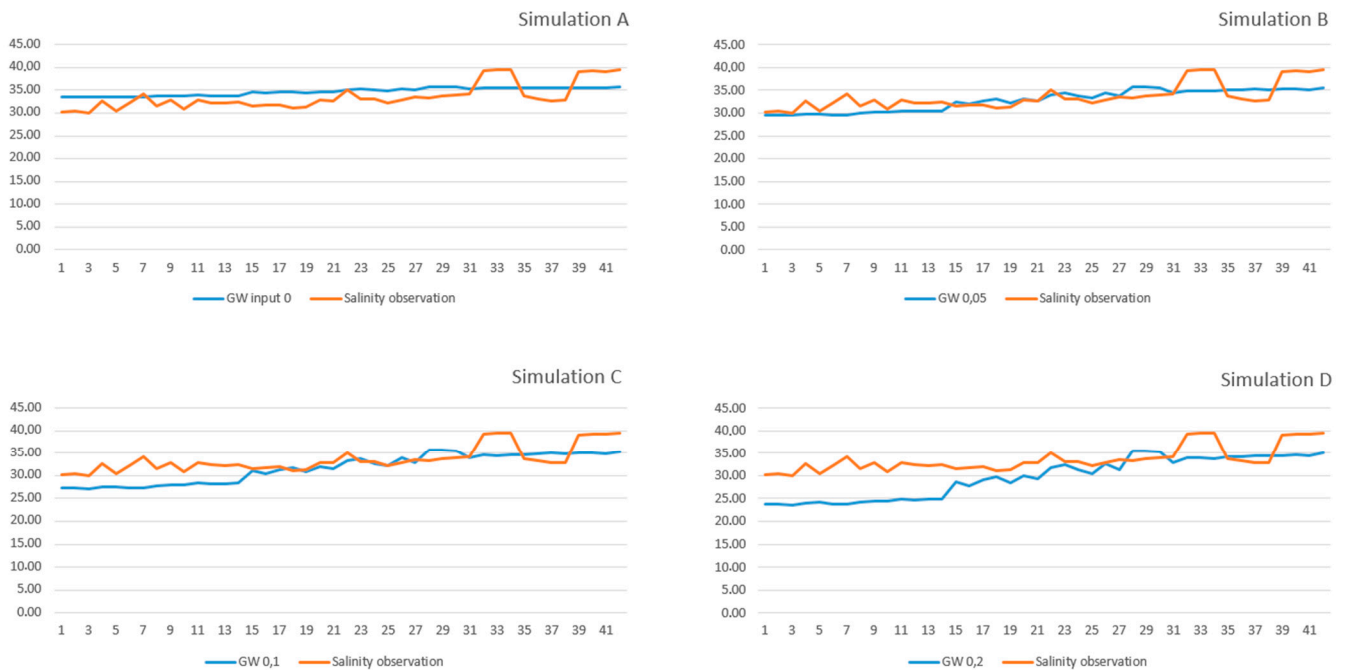


Figure 5. Modeled and observed salinity (PSU) comparison for each SGD input case (Simulation A): 0; (Simulation B): 0.05; (Simulation C): 0.1; (Simulation D): 0.2. With the *x*-axis representing the stations' numbers and the *y*-axis representing the salinity values.

3.2. Physical Parameters Reproduction

3.2.1. Modeled Salinity

Results shown in (Table A2) correspond to the period of time from 1 March 2013 until 1 April 2013, and the last column of the table presents the observed salinity referring to the study in [26] for the same period.

The average salinity presented in (Figure 6a) corresponds to the spring season starting from February until June 2013, taking into consideration the fresh SGD inputs $0.05 \text{ m}^3 \text{ s}^{-1}$, where the highest modeled salinity is between 35.85 psu and 36.14 psu in the boundary area and in the downstream and slightly in the middle part of the lagoon. The lowest modeled value spotted in the inner and slightly in the middle area is 29.15 psu.

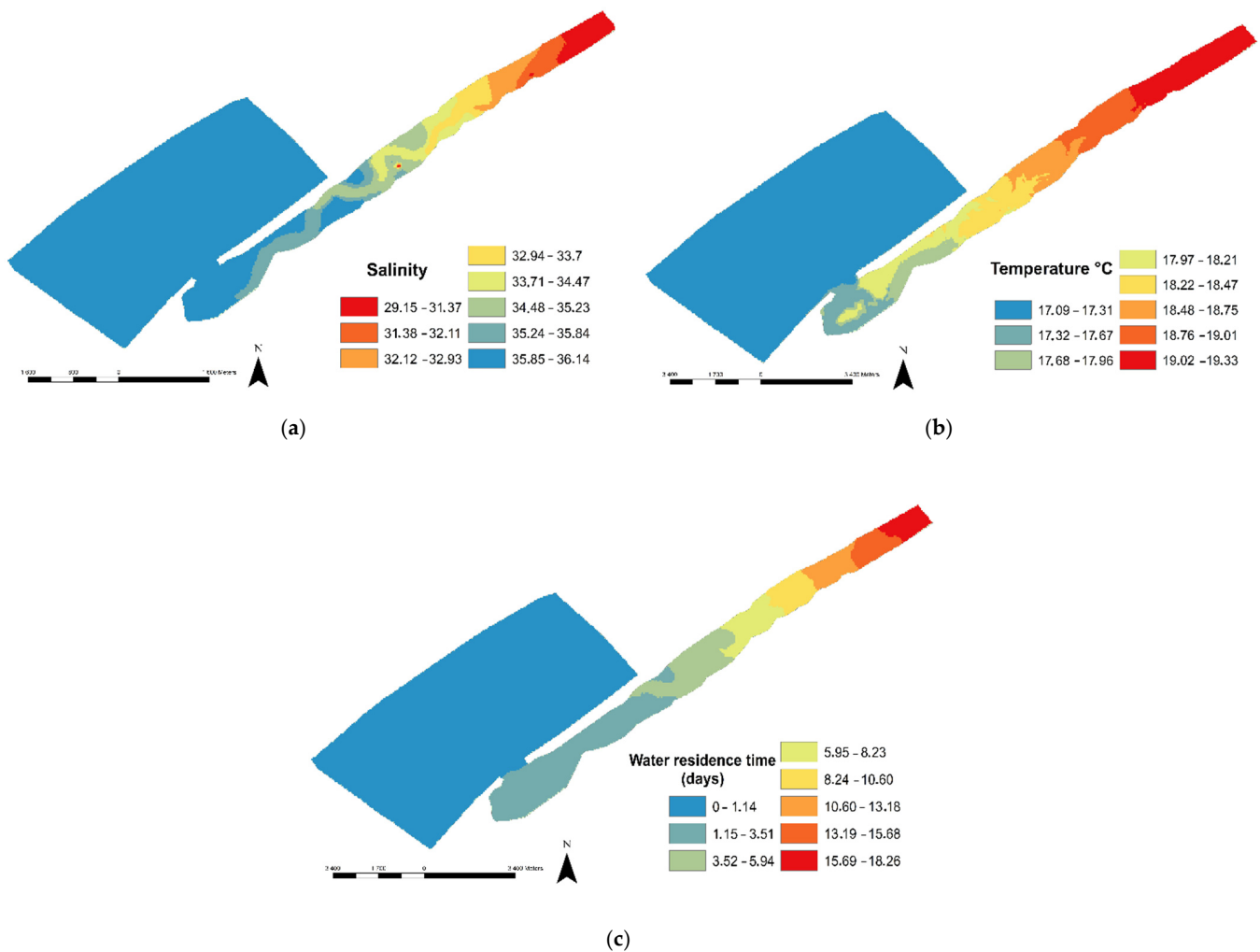


Figure 6. Plots of average modeled physical parameters in Oualidia lagoon for the spring period from February until June 2013. (a) Salinity/PSU. (b) Temperature/°C. (c). WRT/days.

Salinity’s overall results are quite good, and the difference in (Figure 5B) is mainly due to the fact that the exact points of groundwater introduction are not known.

3.2.2. Modeled Water Temperature

The average temperature in (Figure 6b) was modeled for the spring season between February and June 2013. The highest temperature is between 18 to 19 °C, in the inner and the middle parts of the lagoon, while the downstream water temperature is ~17 °C.

As for the annual modeled average temperature for the whole year of 2012, the relatively high-water temperature is in the inner area of the lagoon between 21 and 21.5 °C, while the lower temperature located in the downstream and boundary surface where the inlets is around 19 °C.

3.2.3. Modeled WRT

WRT is defined as the time it takes for every given particle of water to exit a water body throughout its outflow to the sea [34]. The water flushing in the lagoon shown in (Figure 6c) was also modeled for the spring season from February to June 2013. In the downstream of the lagoon near the inlets, the WRT varies from one to three days and a half, in the middle part of the lagoon approximately from five to ten days, while the longest modeled WRT is between ~15 and a half and ~18 days located in the very end of the lagoon in the inner part.

The modeled annual average WRT for the year 2012 showed that the shortest period the water flushing can take inside the lagoon is ~1 to 3 days in the downstream area, while the longest period of time can reach up to ~22 days, while the middle part flushing period varies from ~7 to 12 days. The maximum amount of time of water residency for the year 2012 was modeled during the month of March with ~25 days and a half in the inner part, and the minimum was modeled during the month of December with ~21 h to 2 days and a half in the downstream part and ~15 to 19 days in the inner part.

4. Discussion

4.1. Effect of SGD on Salinity

There are two main sources of water input to the Oualidia lagoon—exchange of the oceanic water from the Atlantic Ocean and SGD flows from a karstic aquifer system. In a recent study from the Oualidia lagoon [2], the salinity gradients and radium concentrations were discussed as a result of SGD mixing and exchange in the lagoon and underground estuary. It was also mentioned that SGD flow rates to the lagoon vary in time depending on climatic, oceanic, and hydrological forcing.

Modeling the spatial salinity distribution in the Oualidia lagoon without considering the SGD inputs produced the salinity gradient opposite to the in-situ observations' highest values in the inner part of the lagoon. In this case, the Oualidia lagoon would have shown the typical features of a hyper-saline lagoon. However, this is not the case. Data shows clearly that salinity decreases from the inlet to the inner parts of the lagoon. With no river flowing into the lagoon, the only explanation is an SGD input that is not accounted for. As is stated in the previous study [6], the Oualidia lagoon is maintained by fresh groundwater inflow, and as a result, salinity decreases going upstream to the lagoon.

With the introduction of freshwater discharge from underwater wells of $0.05 \text{ m}^3 \text{ s}^{-1}$, the salinity gradient in the lagoon was reversed with the highest modeled salinity of 35.51 psu near the lagoon entrance and the lowest modeled salinity of 29.49 psu in the inner part of the lagoon. The lowest modeled salinity without considering SGD inputs was around 33.45 psu. Therefore, fresh SGD discharge, despite its relatively small input, is most definitely influencing the salinity in the lagoon.

Even if the salinity values on the transect are not exactly reproducing the measurements, the average level of salinity is well reproduced. The bias between measured and modeled salinity at individual points could be explained by the fact that only approximate locations of the SGD were available following estimates from the previous study [2]. It is anticipated that with a better knowledge of the discharge locations, spatial prediction of the salinity will be closer to the measured values. So far, our modeled results are the only spatial estimates of the SGD-induced salinity gradients.

Our results are consistent with similar findings in other coastal lagoons in arid or semi-arid areas. In Australia, the SGD discharge into a coastal lagoon off the coast of Perth is responsible for lower surface salinity closer to the coast [37]. In the Celestún lagoon in the Gulf of Mexico, there is a constant salinity gradient ranging from 14 to 19‰ in the inner zone to 36 to 41‰ in the coastal area [38]. Even in areas with more abundant precipitation, SGD could alternate the salinity gradients. In a modeling investigation in Ringkøbing Fjord in Western Jutland, Denmark, the appearance of a very abrupt change in salinity is found to be due to the vertical exaggeration of the aquifer's surface area. Near the beach, SGD discharges into the sea from a terrestrial source, but SGD from deeper sections has mingled with seawater. At the contact, the salinity distribution exhibits an abrupt transition from freshwater to saltwater, forming the distinctive saltwater wedge [39].

4.2. Seasonality Effect on Groundwater Input

Seasonal patterns in precipitation and evaporation are the main factors responsible for the variation in SGD flow over the annual cycle [40]. We expect the seasonal climate changes to contribute to the variation in SGD inputs to the Oualidia lagoon as well. With average yearly precipitation of 372.0 mm, most of it occurs during the period between

September and April, while it could be as low as 0.5 mm in August during the summer. The investigated period (March to July) could be characterized as less than average to dry, and, subsequently, the SGD inputs should be of a lower magnitude than one during the winter period. As we used the constant forcing of the SGD flow to the lagoon and calibrated according to the salinity observed in March (~35 mm/month, roughly the average monthly precipitation for the Oualidia lagoon area), we could expect our salinity distribution results to be representative for the lagoon as average annual values.

However, we could also expect much higher salinities during summer, when not only SGD inputs reduce, but also effective evaporation increases. Such variations are also common in other lagoons. In the Celestún lagoon (Gulf of Mexico), the SGD intake was not consistent since it was affected by rainfall and tide cycles [38]. In the Marina lagoon in Egypt, radon levels, which are an indicator of the SGD inputs, were found to be much greater in spring than in summer, indicating either increased input rates or decreased mixing/atmospheric losses during the rainy season [41].

4.3. Nutrients Provided by SGD Discharge and WRT

Submarine SGD discharge is recognized as an important source not only of freshwater, but also of nutrients to some coastal environments. When collating the modeled monthly WRT values with chemical characteristics of the water column obtained in the previous study [24], there was a strong positive correlation between nitrogen forms (ammonia and nitrates) and temperature, while the correlation with salinity was found to be strongly negative (Figure 7). The elevated concentrations of ammonia in the water of the lagoon in late summer are not directly related to the lagoon flushing, in contrast to the nitrates, which are obviously are of terrestrial (SGD) or lagoon (aquaculture) origin. This is also supported by much lower concentrations of nitrogen compounds in the coastal Atlantic Ocean [24]. As the lagoon has no significant freshwater input sources, the exchange between the lagoon and the Atlantic is the main factor affecting the flushing rate. Therefore, we do not expect the WRT to be influenced by SGD input. Meanwhile, the flushing itself affects the concentrations of nutrients and oxygen, temperature, and salinity, and, subsequently, the water quality, creating a gradient along the lagoon [23,24]. Similar gradients were also observed for the phytoplankton [23].

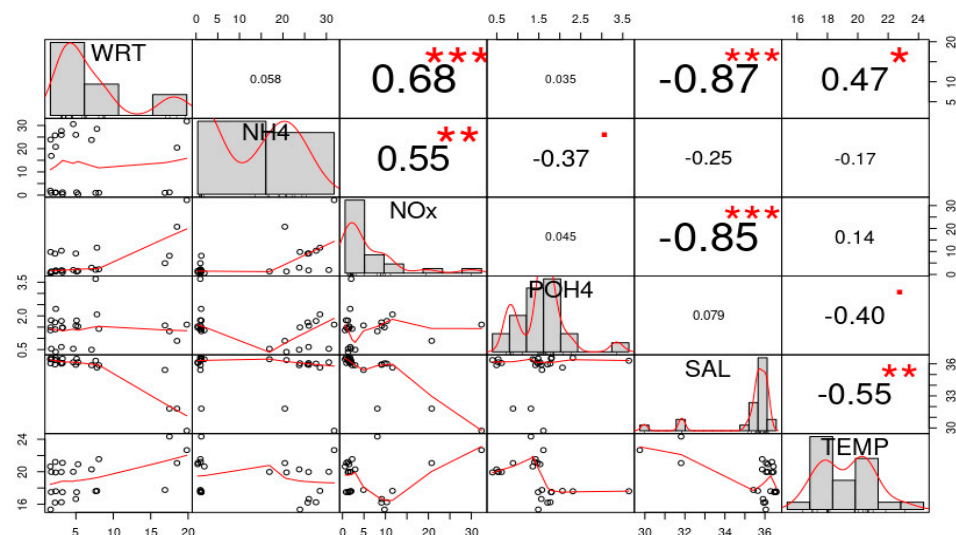


Figure 7. Correlation matrix between monthly WRT and water quality parameters (Ammonium, Nitrate, Phosphate, salinity, temperature) (High tide). The distribution of each variable is shown on the diagonal. On the bottom of the diagonal: the bivariate scatter plots with a fitted line are displayed. On the top of the diagonal: the value of the correlation plus the significance level as stars. Each significance level is associated to a symbol: p -values (0, 0.001, 0.01, 0.05, 0.1, 1) \Leftrightarrow symbols ("***", "**", "*", ".", "", "").

Unfortunately, to our knowledge, there are no data on the nutrient concentrations in SGD inputs to the Oualidia lagoon. However, in general, the quantities of nitrogen and phosphorus (N and P) in SGD are very variable and rely on a variety of factors, including the type of soil and aquifer, permeability, recharge rate, and temperature [42]. SGD inputs in the Marmion lagoon, Australia, the primary source of nitrates and silicates were SGD discharges providing sufficient nitrate to replenish the dissolved nitrate in the lagoon water mass about every eight days. The rate of nitrate-nitrogen supply by SGD inputs exceeds the amount necessary for lagoon macrophyte growth rates [37].

4.4. Physico-Chemical and Biological Gradients in the Lagoon

Calculated spatial distribution of WRT, temperature, and salinity reduced to coordinates in two PCA axes is consistent with lagoon zones developed earlier [26] using the benthic macroinvertebrate distribution (Table 3; Figure 8), showing clear gradients in these three parameters in the transition from the outer marine to the inner estuarine parts of the lagoon.

Table 3. Eigenvalues, the proportion of total variability, as well as correlations between the original variables and the first three principal components (PCs).

Variable	PC1	PC2
Salinity	0.990	−0.122
WRT	−0.986	0.156
Temperature	−0.958	−0.286
Eigenvalue	2.869	0.121
Variance contribution (%)	95.64	4.04
Cumulative variance contribution rate (%)	95.6	99.7

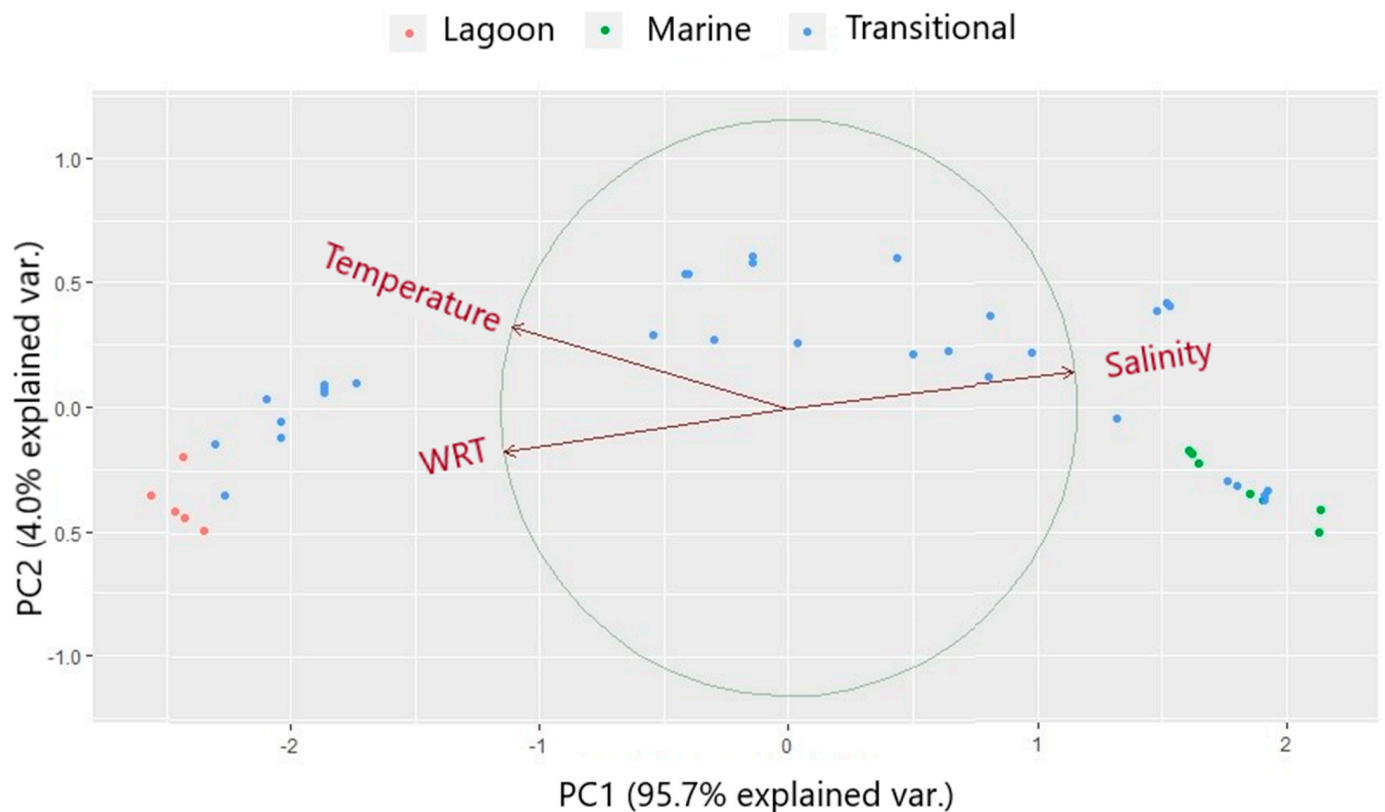


Figure 8. Biplots and distribution of sampling locations across the first two axes of principal components. Colors represent the assignment of sampling points to benthic zonation according to [26].

4.5. WRT Relevance to the Oyster Farming in Oualidia

Oyster farming as the main aquaculture activity in the lagoon of Oualidia. It is also one of the main reasons why the lagoon has a touristic reputation. There are ten existing aquaculture farms in Oualidia (Table 4). Their annual production is estimated to be around ~254 t/year. The farm (1) is located where the minimum WRT was modeled for the year 2012, while the farm (10) is located in the inner part of the lagoon (Figure 9a) (Table 4).

Table 4. Aquaculture activity distribution of farms oyster locations, production and the MIN, max and average WRT in their concession locations.

Oyster Farms	Purifications Station	Minimum WRT	Maximum WRT	Average WRT
Bennaser (1)	✓	2.912901	2.92307	2.917986
Rhouane (2)	✓	2.968186	2.974259	2.971223
Ostrea (3)	✓	3.107552	7.579004	4.321887
Alaoui (4)	✓	3.36252	3.613524	3.48225
Wifak (5)	×	3.67748	3.778902	3.733497
Kinan (6)	×	3.876138	4.746943	4.289131
Saidi (7)	✓	2.72293	6.702939	4.987685
Princesse (8)	✓	2.999807	7.076069	5.203157
Kinan junior (9)	×	3.788272	4.099238	3.889388
Cooperative feminine (10)	×	7.027832	8.41517	7.760968

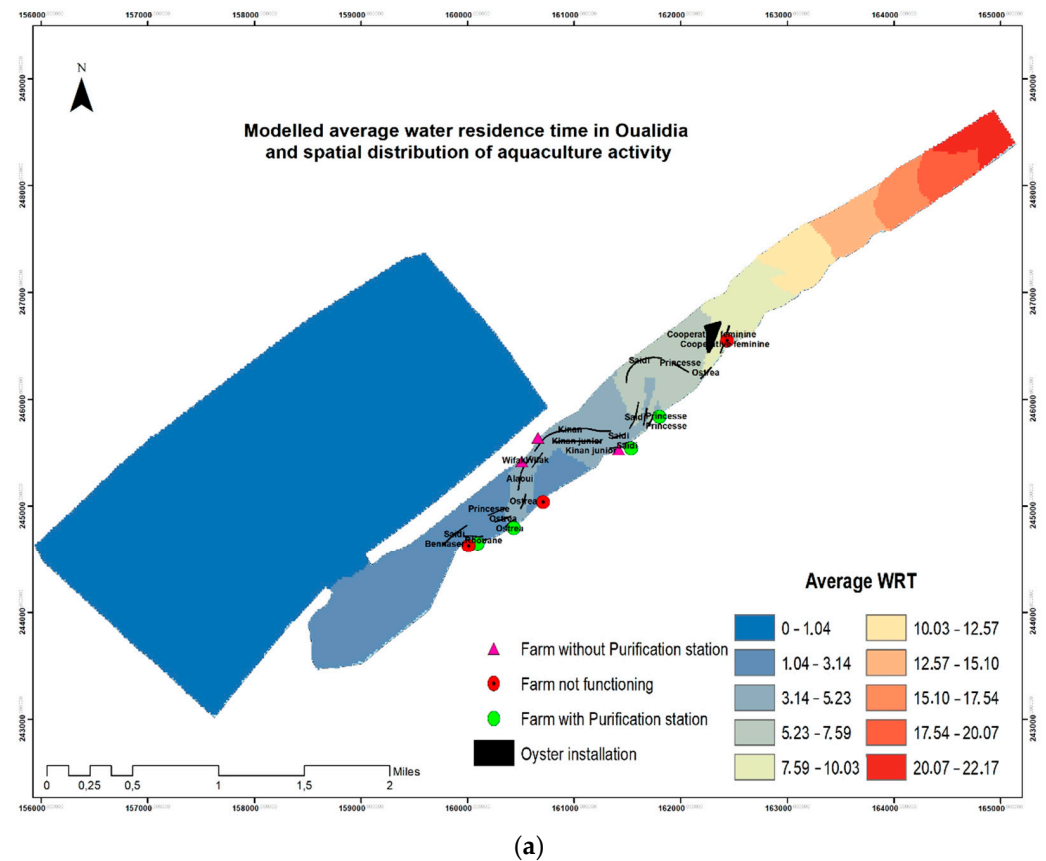


Figure 9. Cont.

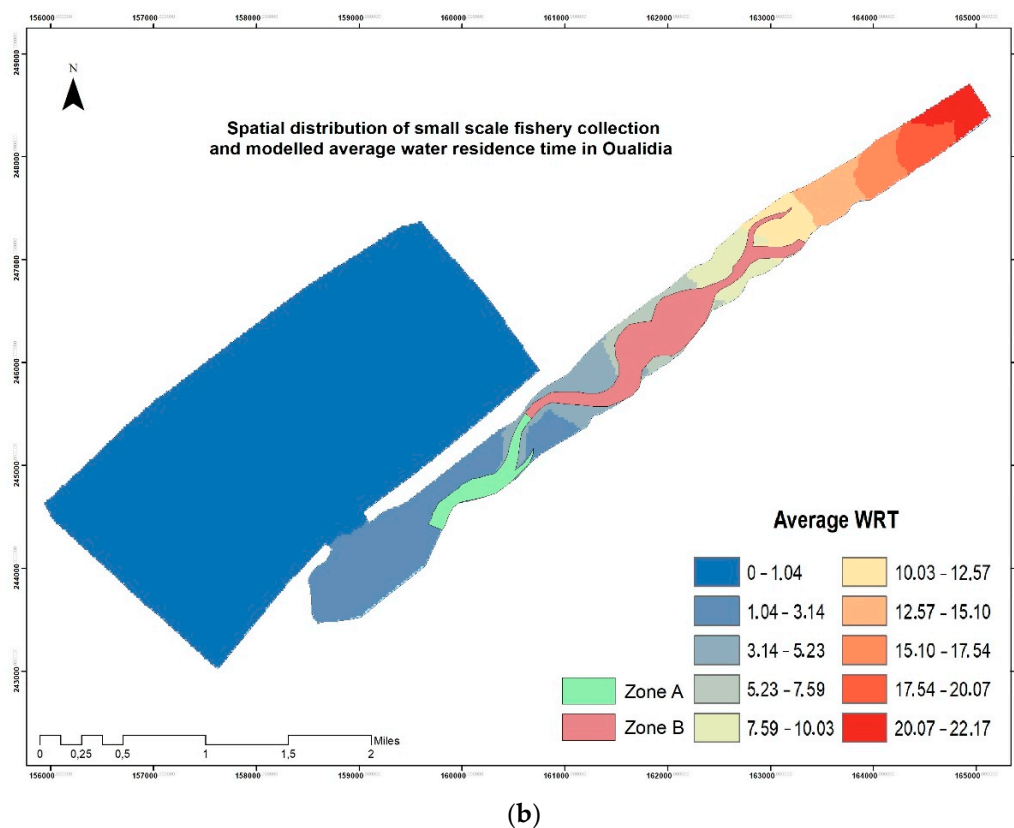


Figure 9. (a) Modeled average WRT in days in Oualidia lagoon for the year 2012 and spatial distribution of aquaculture activity; (b) Spatial distribution of zones of collection of invertebrates' activity and modeled average WRT in Oualidia lagoon for the year 2012.

It has been shown that sites impacted by fresh SGD offer favorable circumstances for mussel and oyster development. Similarly, improved growth rate and a number of fish have been demonstrated in relation to fresh SGD locations, with implications for small-scale fishing [43].

The placement of the aquaculture facilities must regard both WRT and, subsequently, dissolved inorganic nitrogen concentrations in the lagoon. The official designation of the two aquaculture zones (with or without the requirement to let oysters be kept in some kind of purification facility before being delivered to the supplier) (Figure 9b) generally correlate well with the WRT map, but still more detailed spatial designation schemes might be needed to address the gradients of flushing and water quality existing in the lagoon.

5. Conclusions

The application of the SHYFEM model to the Oualidia lagoon has revealed the importance of groundwater inputs, which are critical to the distribution of the salinity between the inner and outer parts of the lagoon.

The spatial distribution of WRT, however, depends mostly exclusively on tidal flushing. However, the lack of data on nutrient content in SGD, the positive correlation between nitrate concentrations and WRT, and the negative relationship between salinity and nitrates point toward possible inputs of inorganic nitrogen from groundwater sources into the lagoon. This factor must be considered when planning aquaculture activities in the lagoon, and full nutrient balance should be calculated.

The model-calculated gradients of physical parameters correspond well to the benthic zonation in the lagoon developed in previous studies. It allows using future projections of climatic changes based on the variation of physical forcing variables as a proxy to biological changes in the future.

Author Contributions: Conceptualization, S.E., G.U. and A.R.-B.; Methodology, S.E. and G.U.; Software, S.E., G.U., F.M. and J.M.; Formal analysis, S.E. and A.R.-B.; Investigation, S.E.; Data curation, S.E., M.M. and K.H.; Writing—original draft preparation, S.E.; Writing—review and editing, S.E., G.U., M.M., F.M., J.M. and A.R.-B.; Visualization, S.E. and A.R.-B.; Supervision, G.U. and A.R.-B. All authors have read and agreed to the published version of the manuscript.

Funding: This research received no external funding.

Institutional Review Board Statement: Not applicable.

Informed Consent Statement: Not applicable.

Data Availability Statement: Not applicable.

Acknowledgments: Bathymetry and tide gauges' stations data used in this study were provided by the DPDPM (Morocco). We would like to thank the anonymous reviewers and the editor for their valuable comments and remarks that helped us to improve the original manuscript.

Conflicts of Interest: The authors declare no conflict of interest.

Appendix A

Table A1. Modeled and observed comparison for phase and amplitude in station 1, 2, 3, 4, and 5.

	Station 1				Station 2				Station 3				Station 4				Station 5			
	Phase		Amp		Phase		Amp		Phase		Amp		Phase		Amp		Phase		Amp	
	Measured	Modeled	Measured	Modeled																
Q1	245	255.63	0.02	0.0216	268	272.95	0.02	0.0169	281	276.32	0.02	0.0163	278	271.70	0.01	0.0118	313	293.69	0.01	0.0116
O1	302	306.77	0.06	0.0615	323	330.58	0.06	0.059	333	337.12	0.06	0.059	333	351.74	0.06	0.0487	347	352.65	0.03	0.0332
NO1	196	45.71	0	0.0062	55	16.11	0.01	0.0035	Ns	31.71	Ns	0.0033	47	194.33	0.01	0.0038	150	143.06	0.01	0.0008
P1	51	45.04	0.03	0.0211	74	66.65	0.02	0.0203	95	72.56	0.02	0.02	110	66.60	0.02	0.0099	87	59.44	0.03	0.0099
K1	44	50.77	0.09	0.0696	67	72.19	0.06	0.065	88	78.41	0.06	0.0647	103	91.58	0.07	0.0487	79	95.07	0.08	0.0333
MU2	26	329.96	0.04	0.0006	179	191.09	0.03	0.0558	166	188.59	0.05	0.0636	208	216.68	0.01	0.0113	112	75.87	0.09	0.0641
N2	29	35.43	0.2	0.2099	66	58.14	0.15	0.1449	78	69.83	0.15	0.1467	74	81.06	0.25	0.0895	110	100.69	0.48	0.2081
M2	49	51.72	0.96	0.9745	87	69.22	0.8	0.7925	77	77.72	0.79	0.7917	73	94.81	0.76	0.4364	250	267.24	0.02	0.0163
L2	135	209.73	0.01	0.0003	357	38.93	0.04	0.025	3	35.37	0.04	0.0295	49	53.94	0.01	0.0067	144	123.14	0.16	0.0999
S2	62	76.83	0.32	0.3437	94	100.06	0.27	0.2319	109	112.79	0.26	0.2326	107	124.65	0.23	0.1397	166	128.59	0.04	0.0318
K2	85	72.24	0.09	0.0967	117	100.69	0.07	0.0694	131	113.74	0.07	0.0709	123	127.78	0.05	0.0459	166	168.81	0.02	0.0215
MK3	288	73.11	0	0.0002	56	42.07	0.01	0.0172	54	48.07	0.01	0.0139	47	123.85	0.01	0.0184	180	154.64	0.05	0.0446
MN4	92	74.10	0.01	0.0005	52	43.17	0.04	0.0529	66	58.58	0.03	0.0424	62	115.93	0.03	0.0453	179	181.63	0.13	0.1014
M4	149	149.05	0.01	0.0153	68	58.84	0.08	0.1165	76	75.16	0.08	0.0903	73	136.50	0.08	0.1226	339	344.47	0.01	0.0172
SN4	210	354.62	0	0.0001	115	291.94	0.02	0.02	127	311.49	0.01	0.0211	208	333.70	0.02	0.0166	211	200.68	0.1	0.0719
MS4	231	145.90	0.01	0.0009	94	87.13	0.08	0.0893	106	104.56	0.06	0.0746	105	158.51	0.06	0.0769	201	206.71	0.01	0.0126
S4	283	262.16	0	0.0004	141	136.21	0.02	0.0161	148	152.82	0.02	0.0159	190	182.94	0.01	0.0134	224	245.31	0.03	0.0471
M6	40	198.15	0	0.0001	ns	39.56	Ns	0.0107	Ns	57.58	Ns	0.0097	177	175.37	0.06	0.0418	254	267.60	0.04	0.0492
2MS6	111	220.90	0	0.0002	334	57.91	0.02	0.0134	353	88.26	0.01	0.0117	203	207.01	0.03	0.0415	313	293.69	0.01	0.0116

Table A2. Modeled salinity (PSU) in 42 stations for each estimated SGD input scenario.

Transects	Stations	SGD 0	SGD 0.05	SGD 0.1	SGD 0.2	Observation
Transect A	S1	33.52	29.59	27.27	23.69	30.17
	S2	33.51	29.57	27.25	23.68	30.36
	S3	33.45	29.49	27.19	23.63	30.08
	S4	33.63	29.82	27.55	24.05	32.56
	S5	33.62	29.84	27.59	24.10	30.33
	S6	33.52	29.66	27.36	23.85	32.12
	S7	33.49	29.57	27.26	23.70	34.15
	S8	33.70	30.07	27.82	24.24	31.61
	S9	33.69	30.12	27.91	24.40	32.81
	S10	33.68	30.12	27.91	24.45	30.78
	S11	33.91	30.54	28.41	24.98	32.81
	S12	33.85	30.40	28.21	24.73	32.31
	S13	33.83	30.42	28.27	24.83	32.24
	S14	33.81	30.43	28.31	24.90	32.43
Transect B	S15	34.55	32.47	31.05	28.74	31.61
	S16	34.43	32.03	30.44	27.71	31.67
	S17	34.60	32.70	31.40	29.06	31.86
	S18	34.73	32.99	31.79	29.80	31.16
	S19	34.52	32.28	30.79	28.38	31.23
	S20	34.75	33.13	32.01	30.08	32.81
	S21	34.67	32.74	31.44	29.28	32.75
	S22	35.09	34.02	33.26	31.83	35.04
	S23	35.25	33.35	33.68	32.48	33.01
	S24	35.00	33.66	32.73	31.20	33.13
	S25	34.87	33.30	32.24	30.46	32.12
	S26	35.30	34.49	33.91	32.70	32.88
	S27	35.02	33.73	32.85	31.35	33.58
Transect C	S28	35.74	35.67	35.63	35.53	33.26
	S29	35.74	35.67	35.63	35.53	33.70
	S30	35.69	35.53	35.42	35.40	34.02
	S31	35.29	34.47	33.91	32.92	34.28
	S32	35.45	34.91	34.53	33.86	39.30
	S33	35.45	34.89	34.51	33.85	39.49
	S34	35.45	34.90	34.52	33.81	39.43
	S35	35.51	35.05	34.73	34.16	33.77
	S36	35.53	35.10	34.80	34.22	33.20
	S37	35.59	35.27	35.04	34.40	32.75
	S38	35.55	35.15	34.88	34.37	32.88
	S39	35.58	35.24	35.01	34.36	39.05
	S40	35.57	35.22	34.97	34.53	39.36
	S41	35.56	35.20	34.94	34.49	39.17
	S42	35.68	35.51	35.39	35.11	39.49

References

1. Newton, A.; Brito, A.C.; Icely, J.D.; Derolez, V.; Clara, I.; Angus, S.; Schernewski, G.; Inácio, M.; Lillebø, A.I.; Sousa, A.I.; et al. Assessing, quantifying and valuing the ecosystem services of coastal lagoons. *J. Nat. Conserv.* **2018**, *44*, 50–65. [\[CrossRef\]](#)
2. Fakir, Y.; Claude, C.; El Himer, H. Identifying groundwater discharge to an Atlantic coastal lagoon (Oualidia, Central Morocco) by means of salinity and radium mass balances. *Environ. Earth Sci.* **2019**, *78*, 626. [\[CrossRef\]](#)
3. Hilmi, K.; Orbi, A.; Lakhdar, J.I.; Sarf, F. Etude courantologique de la lagune de Oualidia (Maroc) en automne. *Bull. L'Inst. Sci. Rabat Sect. Sci. Vie* **2005**, *26–27*, 67–71.
4. Hilmi, K.; Orbi, A.; Lakhdar, J.I. Hydrodynamisme de la lagune de Oualidia (Maroc) durant l'été et l'automne 2005. *Bull. L'Inst. Sci. Rabat Sect. Sci. Terre* **2009**, *31*, 29–34.
5. Maanan, M.; Ruiz-fernandez, A.C.; Maanan, M.; Fattal, P.; Zourarah, B.; Sahabi, M. A long-term record of land use change impacts on sediments in Oualidia lagoon, Morocco. *Int. J. Sediment Res.* **2014**, *29*, 10. [\[CrossRef\]](#)
6. Hilmi, K.; Koutitonsky, V.G.; Orbi, A.; Lakhdar, J.I.; Chagdali, M. Oualidia lagoon, Morocco: An estuary without a river. *Afr. J. Aquat. Sci.* **2005**, *30*, 1–10. [\[CrossRef\]](#)

7. Rharbi, N.; Ramdani, M.; Berraho, A.; Idrissi, A.L. Caractéristiques hydrologiques et écologiques de la lagune de Oualidia, milieu paralique de la côte atlantique marocaine. *Mar. Life* **2001**, *11*, 3–9.
8. García-Oliva, M.; Pérez-Ruzafa, Á.; Umgiesser, G.; McKiver, W.; Ghezzi, M.; De, P.F.; Concepción, M. Assessing the Hydrodynamic Response of the Mar Menor Lagoon to Dredging Inlets Interventions through Numerical Modelling. *Water* **2018**, *10*, 959. [[CrossRef](#)]
9. Umgiesser, G.; Canu, D.M.; Cucco, A.; Solidoro, C. A finite element model for the Venice Lagoon. Development, set up, calibration and validation. *J. Mar. Syst.* **2004**, *51*, 123–145. [[CrossRef](#)]
10. Holtermann, P.; Burchard, H.; Jennerjahn, T. Hydrodynamics of the Segara Anakan Lagoon. *Reg. Environ. Chang.* **2009**, *9*, 245–258. [[CrossRef](#)]
11. Duque, C.; Jessen, S.; Tirado-Conde, J.; Karan, S.; Engesgaard, P. Application of Stable Isotopes of Water to Study Coupled Submarine Groundwater Discharge and Nutrient Delivery. *Water* **2019**, *11*, 1842. [[CrossRef](#)]
12. Rodellas, V.; Garcia-Orellana, J.; Masqué, P.; Feldman, M.; Weinstein, Y. Submarine groundwater discharge as a major source of nutrients to the Mediterranean Sea. *Proc. Natl. Acad. Sci. USA* **2015**, *12*, 3926–3930. [[CrossRef](#)]
13. Müller, S.; Jessen, S.; Sonnenborg, T.O.; Meyer, R.; Engesgaard, P. Simulation of density and flow dynamics in a lagoon aquifer environment and implications for nutrient delivery from land to sea. *Front. Water* **2021**, *3*, 165. [[CrossRef](#)]
14. Menció, A.; Casamitjana, X.; Mas-Pla, J.; Coll, N.; Compte, J.; Martinoy, M.; Pascual, J.; Quintana, X.D. Groundwater dependence of coastal lagoons: The case of La Pletera salt marshes (NE Catalonia). *J. Hydrol.* **2017**, *552*, 793–806. [[CrossRef](#)]
15. Sadat-Noori, M.; Santos, I.R.; Tait, D.R.; McMahan, A.; Kadel, S.; Maher, D.T. Intermittently Closed and Open Lakes and/or Lagoons (ICOLs) as groundwater-dominated coastal systems: Evidence from seasonal radon observations. *J. Hydrol.* **2016**, *535*, 612–624. [[CrossRef](#)]
16. Rapaglia, J.; Ferrarin, C.; Zaggia, L.; Moore, W.S.; Umgiesser, G.; Garcia-Solsona, E.; Garcia-Orellana, J.; Masque, P. Investigation of residence time and groundwater flux in Venice Lagoon: Comparing radium isotope and hydrodynamical models. *J. Environ. Radioact.* **2010**, *101*, 571–581. [[CrossRef](#)] [[PubMed](#)]
17. Umgiesser, G.; Ferrarin, C.; Cucco, A.; De Pascalis, F.; Bellafiore, D.; Ghezzi, M.; Bajo, M. Comparative hydrodynamics of 10 Mediterranean lagoons by means of numerical modeling. *J. Geophys. Res. Ocean.* **2014**, *119*, 2212–2226. [[CrossRef](#)]
18. Ferrarin, C.; Razinkovas-Baziukas, A.; Gulbinskas, S.; Umgiesser, G.; Bliūdžiūtė, L. Hydraulic Regime-Based Zonation Scheme of the Curonian Lagoon. *Hydrobiologia* **2008**, *611*, 133–146. [[CrossRef](#)]
19. Kolarski, T.; Zima, P.; Szydłowski, M. Mathematical Modeling of Ice Thrusting on the Shore of the Vistula Lagoon (Baltic Sea) and the Proposed Artificial Island. *Water* **2019**, *11*, 2297. [[CrossRef](#)]
20. Mejjad, N.; Laissaoui, A.; El-Hammoumi, O.; Benmansour, M.; Benbrahim, S.; Bounouira, H.; Benkdad, A.; Bouthir, F.Z.; Fekri, A.; Bounakhla, M. Sediment geochronology and geochemical behavior of major and rare earth elements in the Oualidia Lagoon in the western Morocco. *J. Radioanal. Nucl. Chem.* **2016**, *309*, 1133–1143. [[CrossRef](#)]
21. Bidet, J.C.; Carruesco, C. Étude sédimentologique de la lagune de Oualidia (Maroc). *Oceanol. Acta* **1982**, *8–14*, 29–37.
22. Bennouna, A.; Berland, B.; El Attar, J.; Assobhei, O. Eau colorée à Lingulodinium polyedrum (Stein) Dodge, dans une zone aquacole du littoral du Doukkala (Atlantique marocain) Lingulodinium polyedrum (Stein) Dodge red tide in shellfish areas along Doukkala coast (Moroccan Atlantic). *Oceanol. Acta* **2002**, *25*, 159–170. [[CrossRef](#)]
23. Somoue, L.; Demarcq, H.; Makaoui, A.; Hilmi, K.; Ettahiri, O.; Ben Mhamed, A.; Agouzouk, A.; Baibai, T.; Larissi, J.; Charib, S.; et al. Influence of Ocean–Lagoon exchanges on spatio-temporal variations of phytoplankton assemblage in an Atlantic Lagoon ecosystem (Oualidia, Morocco). *Reg. Stud. Mar. Sci.* **2020**, *40*, 101512. [[CrossRef](#)]
24. Damsiri, Z.; Natij, L.; Khalil, K.; Loudiki, M.; Rabouille, C.; Ettahiri, O.; Bougadir, B.; Elkalay, K. Spatio-temporal nutrients variability in the Oualidia lagoon (Atlantic Moroccan coast). *Int. J. Adv. Res.* **2014**, *2*, 609–618.
25. Khomalli, Y.; Elyaaougubi, S.; Maanan, M.; Razinkova-Baziukas, A.; Rhinane, H.; Maanan, M. Using Analytic Hierarchy Process to Map and Quantify the Ecosystem Services in Oualidia Lagoon, Morocco. *Wetlands* **2020**, *40*, 2123–2137. [[CrossRef](#)]
26. El Asri, F.; Zidane, H.; Maanan, M.; Tamsouri, M.; Errhif, A. Taxonomic diversity and structure of the molluscan fauna in Oualidia lagoon (Moroccan Atlantic coast). *Environ. Monit. Assess.* **2015**, *187*, 545. [[CrossRef](#)]
27. Zemlys, P.; Ferrarin, C.; Umgiesser, G.; Gulbinskas, S.; Bellafiore, D. Investigation of saline water intrusions into the Curonian Lagoon (Lithuania) and two-layer flow in the Klaipeda Strait using finite element hydrodynamic model. *Ocean Sci.* **2013**, *9*, 573–584. [[CrossRef](#)]
28. Wang, J.D.; Connor, J.J. Chapter 13. In *Mathematical Modeling of Near Coastal Circulation*; Massachusetts Institute of Technology: Massachusetts, MA, USA, 1975.
29. Lynch, D.R.; Werner, F.E. Three-dimensional hydrodynamics on finite elements. Part I: Linearized harmonic model. *Int. J. Numer. Methods Fluids* **1987**, *7*, 871–909. [[CrossRef](#)]
30. Maicu, F.; Abdellaoui, B.; Bajo, M.; Chair, A.; Hilmi, K.; Umgiesser, G. Modelling the water dynamics of a tidal lagoon: The impact of human intervention in the Nador Lagoon (Morocco). *Cont. Shelf Res.* **2021**, *228*, 104535. [[CrossRef](#)]
31. Darwish, M.S.; Moukalled, F. TVD schemes for unstructured grids. *Int. J. Heat Mass Trans.* **2003**, *46*, 599–611. [[CrossRef](#)]
32. Smagorinsky, J. General circulation experiments with the primitive equations, I. The basic experiment. *Mon. Weather Rev.* **1963**, *91*, 99–164. [[CrossRef](#)]
33. Ferrarin, C.; Umgiesser, G. Hydrodynamic modelling of a coastal lagoon: The Cabras lagoon in Sardinia, Italy. *Ecol. Model.* **2005**, *188*, 340–357. [[CrossRef](#)]
34. Cucco, A.; Umgiesser, G. Modeling the Venice Lagoon residence time. *Ecol. Model.* **2006**, *193*, 34–51. [[CrossRef](#)]

35. Takeoka, H. Fundamental concepts of exchange and transport time scales in a coastal sea. *Shelf Res.* **1984**, *3*, 311–326. [[CrossRef](#)]
36. Burau, J.R.; Simpson, M.R.; Cheng, R.T. Data analysis. In *Book Tidal and Residual Currents Measured by an Acoustic Doppler Current Profiler at the West End of Carquinez Strait, San Francisco Bay, California, March to November 1988*; Hirsch, R.M., Ed.; US Geological Survey: Sacramento, CA, USA, 1993; Volume 92, No. 4064.
37. Johannes, R.E.; Hearn, C.J. The Effect of Submarine Groundwater Discharge on Nutrient and Salinity Regimes in a Coastal Lagoon off Perth, Western Australia. *Estuar. Coast. Shelf Sci.* **1985**, *21*, 789–800. [[CrossRef](#)]
38. Herrera-Silveira, J.A. Salinity and nutrients in a tropical coastal lagoon with groundwater discharges to the Gulf of Mexico. *Hydrobiologia* **1996**, *321*, 165–176. [[CrossRef](#)]
39. Haider, K.; Engesgaard, P.; Sonnenborg, T.O.; Kirkegaard, C. Numerical modeling of salinity distribution and submarine groundwater discharge to a coastal lagoon in Denmark based on airborne electromagnetic data. *Hydrogeol. J.* **2015**, *23*, 217–233. [[CrossRef](#)]
40. Kelly, R.P.; Moran, S.B. Seasonal changes in groundwater input to a well-mixed estuary estimated using radium isotopes and implications for coastal nutrient budgets. *Limnol. Oceanogr.* **2002**, *47*, 1796–1807. [[CrossRef](#)]
41. El-Gamal, A.A.; Peterson, R.N.; Burnett, W.C. Detecting Freshwater Inputs via Groundwater Discharge to Marina Lagoon, Mediterranean Coast, Egypt. *Estuaries Coasts* **2012**, *35*, 1486–1499. [[CrossRef](#)]
42. Slomp, C.P.; Van Cappellen, P. Nutrient inputs to the coastal ocean through submarine groundwater discharge: Controls and potential impact. *J. Hydrol.* **2004**, *295*, 64–86. [[CrossRef](#)]
43. Santos, I.R.; Chen, X.; Lecher, A.L.; Sawyer, A.H.; Moosdorf, N.; Rodellas, V.; Tamborski, J.; Cho, H.M.; Dimova, N.; Sugimoto, R.; et al. Submarine groundwater discharge impacts on coastal nutrient biogeochemistry. *Nat. Rev. Earth Environ.* **2021**, *2*, 307–323. [[CrossRef](#)]